

New Inflation vs. Chaotic Inflation, higher degree potentials and the Reconstruction Program in light of WMAP3

D. Boyanovsky,^{1,2,3,*} H. J. de Vega,^{3,2,1,†} C. M. Ho,^{1,‡} and N. G. Sanchez^{2,§}

¹*Department of Physics and Astronomy, University of Pittsburgh, Pittsburgh, Pennsylvania 15260, USA*

²*Observatoire de Paris, LERMA. Laboratoire Associé au CNRS UMR 8112.
61, Avenue de l'Observatoire, 75014 Paris, France.*

³*LPTHE, Université Pierre et Marie Curie (Paris VI) et Denis Diderot (Paris VII),
Laboratoire Associé au CNRS UMR 7589, Tour 24,
5ème. étage, 4, Place Jussieu, 75252 Paris, Cedex 05, France*

(Dated: August 3, 2021)

The CMB power spectra are studied for different *families* of single field new and chaotic inflation models in the effective field theory approach to inflation. We implement a systematic expansion in $1/N_e$ where $N_e \sim 50$ is the number of e-folds before the end of inflation. We study the dependence of the observables (n_s , r and $dn_s/d \ln k$) on the degree of the potential ($2n$) and confront them to the WMAP3 and large scale structure data: This shows in general that fourth degree potentials ($n = 2$) provide the best fit to the data; the window of consistency with the WMAP3 and LSS data narrows for growing n . New inflation yields a good fit to the r and n_s data in a wide range of field and parameter space. Small field inflation yields $r < 0.16$ while large field inflation yields $r > 0.16$ (for $N_e = 50$). All members of the new inflation family predict a small but negative running $-4(n+1) \times 10^{-4} \leq dn_s/d \ln k \leq -2 \times 10^{-4}$. (The values of r , n_s , $dn_s/d \ln k$ for arbitrary N_e follow by a simple rescaling from the $N_e = 50$ values). A reconstruction program is carried out suggesting quite generally that for n_s consistent with the WMAP3 and LSS data and $r < 0.1$ the **symmetry breaking scale** for new inflation is $|\phi_0| \sim 10 M_{Pl}$ while the **field scale** at Hubble crossing is $|\phi_c| \sim M_{Pl}$. The family of chaotic models feature $r \geq 0.16$ (for $N_e = 50$) and only a *restricted subset* of chaotic models are consistent with the combined WMAP3 bounds on r , n_s , $dn_s/d \ln k$ with a narrow window in field amplitude around $|\phi_c| \sim 15 M_{Pl}$. We conclude that a measurement of $r < 0.16$ (for $N_e = 50$) distinctly rules out a large class of chaotic scenarios and favors small field new inflationary models. As a general consequence, **new inflation** emerges more favoured than chaotic inflation.

I. INTRODUCTION

Inflation provides a simple and robust mechanism to solve several outstanding problems of the standard Big Bang model [1, 2] becoming a leading paradigm in cosmology. Superhorizon quantum fluctuations amplified during inflation provide an explanation of the origin of the temperature anisotropies in the cosmic microwave background (CMB) and the seeds for large scale structure formation[3], as well as of tensor perturbations (primordial gravitational waves). Although there is a diversity of inflationary models, most of them predict fairly generic features: a gaussian, nearly scale invariant spectrum of (mostly) adiabatic scalar and tensor primordial fluctuations [3]. These features provide an excellent fit to the highly precise data provided by the Wilkinson Microwave Anisotropy Probe (WMAP) [4, 5, 6, 7] which begins to constrain inflationary models.

The combination of CMB [5, 6] and large scale structure data [8, 9] yield fairly tight constraints for the two dimensional marginalized contours of the tensor to scalar ratio r and the scalar index n_s . While $n_s = 1$ was excluded at the 95%*CL* in [9] a most notable result that stems from the analysis of WMAP3 data is a confirmation that a scale invariant Harrison-Zeldovich spectrum is excluded at the 3σ level [6]. A combination of data from WMAP3 and large scale surveys distinctly favor $n_s < 1$ [10]. These latest bounds on the index of the power spectrum of scalar perturbations, and emerging bounds on the ratio of tensor to scalar fluctuations r begin to offer the possibility to discriminate different inflationary models. For example, the third year WMAP data disfavors the predictions for the scalar index and the tensor to scalar ratio from a monomial inflationary potential $\lambda \phi^4$ showing them to lie outside

*Electronic address: boyan@pitt.edu

†Electronic address: devega@lpthe.jussieu.fr

‡Electronic address: cmho@phyast.pitt.edu

§Electronic address: Norma.Sanchez@obspm.fr

the 3σ contour, but the simple monomial $m^2 \phi^2/2$ yields a good fit to the data [6] and predicts a tensor to scalar ratio $r \sim 0.16$ within the range of forthcoming CMB observations.

Current and future CMB observations in combination with large scale structure surveys will yield tight constraints on the inflationary models, this motivates the exploration of clear predictions from the models and their confrontation with the data.

In distinction with the approach followed in [5, 6, 11] or studies of specific models[12], or statistical analysis combined with WMAP3 and LSS data[13, 14], we study the predictions for the power spectra of scalar fluctuations and the tensor to scalar ratio for *families* of new and chaotic inflationary models in the framework of the method presented in ref.[15]. This method relies on the effective field theory approach combined with a systematic expansion in $1/N_e$ where $N_e \sim 50$ is the number of e-folds before the end of inflation. The family of inflationary models that we study is characterized by effective field theories with potentials of the form

$$V(\phi) = V_0 - \frac{1}{2} m^2 \phi^2 + \frac{\lambda}{2n} \phi^{2n} \quad , \quad \text{broken symmetry} \quad (1)$$

$$V(\phi) = \frac{1}{2} m^2 \phi^2 + \frac{\lambda}{2n} \phi^{2n} \quad , \quad \text{unbroken symmetry} \quad , \quad (2)$$

with $n = 2, 3, 4 \dots$. For broken symmetry models with potentials of the form (1) there are two distinct regions: small and large field, corresponding to values of the inflaton field smaller or larger than the symmetry breaking scale respectively.

We implement the systematic expansion in $1/N_e$ where $N_e \sim 50$ is the number of e-folds before the end of inflation when wavelengths of cosmological relevance crossed the Hubble radius[15]. The $1/N_e$ expansion is a powerful and systematic tool that allows to re-cast the slow roll hierarchy as expansion in powers of $1/N_e$ [15]. This expansion allows us to implement a reconstruction program [16] which yields the scale of the inflaton field when modes of cosmological relevance today crossed the Hubble radius during inflation, and in the case of new inflation models also yields the *scale of symmetry breaking*.

We study the dependence of the observables (n_s , r and $dn_s/d \ln k$) on the degree of the inflaton potential ($2n$) for new and chaotic inflation and confront them with the WMAP3 data. This study shows in general that fourth degree potentials ($n = 2$) provide the best fit to the data. We find that new inflation fits the data on an appreciable wider range of the parameters while chaotic inflation does this in a much narrow range. Therefore, amongst the families of inflationary models studied, new inflation emerges as a leading contender in comparison with chaotic inflation. The present analysis confirms the statement that within the framework of effective field theories with polynomial potentials, new inflation is a preferred model reproducing the present data [18, 19, 20].

Main results of this article:

- The region in inflaton field space which is consistent with the marginalized WMAP3 data can be explored in an expansion in $n_s - 1 + 2/N_e$.
- We find that the point $n_s = 1 - 2/N_e = 0.96$, $r = 8/N_e = 0.16$ which is in the region allowed by the WMAP3 analysis[6] belongs both to new inflation models as a limiting point and to the simple chaotic inflation monomial, $m^2 \phi^2/2$. (i) This point describes a region in field and parameter space that separates small fields from large fields, and (ii) is a degeneracy point for the family of models describing both chaotic and new inflation.
- For all members $n = 2, 3, 4, \dots$ of the new inflation family, the small field region yields $r < 0.16$ while the large field region yields $r > 0.16$. All members of the new inflation family predict a small but negative running:

$$-4(n+1) \times 10^{-4} \leq dn_s/d \ln k \leq -2 \times 10^{-4} .$$

This new inflation family features a *large window* of consistency with the WMAP and LSS data for $n = 2$ that narrows for growing n . If forthcoming data on tensor modes pinpoints the tensor to scalar ratio to be $r < 0.1$, we predict that the *symmetry breaking scale* for these models is $\phi_0 \sim 10 M_{Pl}$ and that the scale of the field at which modes of cosmological relevance today cross the Hubble radius is $\phi_c \sim M_{Pl}$.

- Chaotic inflationary models all yield a tensor to scalar ratio $r \geq 0.16$, where the minimum value $r = 0.16$ corresponds to small amplitude of the inflaton and coincides with the value obtained from the monomial $m^2 \phi^2/2$. The combined marginalized data from WMAP3 [6] yields a very small window of field amplitude, around $|\phi_c| \sim 15 M_{Pl}$ within which chaotic models are allowed by the data. These regions become progressively smaller for larger n . Some small regions in field space consistent with the WMAP3 data feature peaks in the running of the scalar index but in the region consistent with the WMAP3 data in chaotic inflation the running is again negligible ($\sim 10^{-3}$). If future observations determine a tensor to scalar ratio $r < 0.16$, this by itself will **rule out** a large family of chaotic inflationary models.

II. EFFECTIVE FIELD THEORY, SLOW ROLL AND $1/N_e$ EXPANSIONS

In the absence of a fundamental microscopic description of inflation, an effective field theory approach, when combined with the slow roll expansion provides a robust paradigm for inflation with predictive power. The reliability of the effective field theory description hinges on a wide separation between the Hubble and Planck scales, and is validated by the bound from temperature fluctuations $H/M_{Pl} < 10^{-5}$ [15].

The slow roll expansion relies on the smallness of a hierarchy of the dimensionless ratios [2, 16, 21],

$$\epsilon_v = \frac{M_{Pl}^2}{2} \left[\frac{V'(\phi)}{V(\phi)} \right]^2, \quad \eta_v = M_{Pl}^2 \frac{V''(\phi)}{V(\phi)}, \quad \xi_v = M_{Pl}^4 \frac{V'(\phi) V'''(\phi)}{V^2(\phi)}. \quad (3)$$

The effective field theory expansion in H/M_{Pl} and the slow roll expansion are independent, the latter can be interpreted as an adiabatic expansion [15] wherein the derivatives of the inflationary potential are small.

The CMB data is consistently described within the slow roll expansion with inflationary potentials of the form [2, 15]

$$V(\phi) = M^4 v \left(\frac{\phi}{M_{Pl}} \right). \quad (4)$$

Within the slow roll approximation the number of e-folds before the end of inflation for which the value of the field is ϕ_{end} is given by

$$N[\phi(t)] = -\frac{1}{M_{Pl}^2} \int_{\phi(t)}^{\phi_{end}} V(\phi) \frac{d\phi}{dV} d\phi. \quad (5)$$

It proves convenient to introduce N_e as the typical number of e-folds before the end of inflation during which cosmologically relevant wavelengths cross the Hubble radius during inflation, and ϕ_c as the value of the inflaton field corresponding to N_e

$$N_e = -\frac{1}{M_{Pl}^2} \int_{\phi_c}^{\phi_{end}} V(\phi) \frac{d\phi}{dV} d\phi. \quad (6)$$

The precise value of N_e is certainly near $N_e = 50$ [2, 17]. We will take the value $N_e = 50$ as a reference baseline value for numerical analysis, but from the explicit expressions obtained in the systematic $1/N_e$ expansion below, it becomes a simple rescaling to obtain results for arbitrary values of N_e [see eq. (10) below].

The form of the potential eq.(4) and the above definition for the number of e-folds, suggests to introduce the following rescaled field variable [15]

$$\phi = \sqrt{N_e} M_{Pl} \chi \quad (7)$$

where the rescaled field χ is dimensionless. Furthermore, it is also convenient to scale N_e out of the potential and write

$$V(\phi) = N_e M^4 w(\chi). \quad (8)$$

With this definition, eq. (6) becomes

$$1 = - \int_{\chi_c}^{\chi_{end}} \frac{w(\chi)}{w'(\chi)} d\chi \quad (9)$$

where the prime stands for derivative with respect to χ , χ_c is the value of χ corresponding to N_e e-folds before the end of inflation, and χ_{end} is the value of χ at the end of inflation.

We emphasize that there is *no* dependence on N_e in the expression (9), therefore χ_c, χ_{end} only depend on the coupling and the degree n . The slow roll parameters then become,

$$\epsilon_v = \frac{1}{2 N_e} \left[\frac{w'(\chi_c)}{w(\chi_c)} \right]^2, \quad \eta_v = \frac{1}{N_e} \frac{w''(\chi_c)}{w(\chi_c)}, \quad \xi_v = \frac{1}{N_e^2} \frac{w'(\chi_c) w'''(\chi_c)}{w^2(\chi_c)}. \quad (10)$$

It is clear from eqs.(9) and (10) that during the inflationary stage when wavelengths of cosmological relevance cross the horizon, it follows that $w(\chi_c), w'(\chi_c) \sim \mathcal{O}(1)$ leading to the slow roll expansion as a consistent expansion in $1/N_e$ [15].

The connection between the slow roll expansion and the expansion in $1/N_e$ becomes more explicit upon introducing a *stretched* dimensionless time variable τ and a dimensionless Hubble parameter h as follows [15]

$$\tau = \frac{M^2 t}{\sqrt{N_e} M_{Pl}} \quad ; \quad h = \frac{M_{Pl} H}{\sqrt{N_e} M^2}. \quad (11)$$

In terms of τ , χ and h the Friedmann equation and the equation of motion for the inflaton become,

$$h^2(\tau) = \frac{1}{3} \left[\frac{1}{2 N_e} \left(\frac{d\chi}{d\tau} \right)^2 + w(\chi) \right],$$

$$\frac{1}{N_e} \frac{d^2\chi}{d\tau^2} + 3 h \frac{d\chi}{d\tau} + w'(\chi) = 0. \quad (12)$$

This equation of motion can be solved in a systematic expansion in $1/N_e$. The definition (7) also makes manifest that χ is a *slowly varying field*, since a change $\Delta\phi \sim M_{Pl}$ in the inflaton field implies a *small* change of the dimensionless field $\Delta\chi \sim 1/\sqrt{N_e}$.

In terms of these definitions, the CMB observables can be written manifestly in terms of the $1/N_e$ expansion. The amplitude of scalar perturbations is given by

$$\Delta_{\mathcal{R}}^2 = \frac{N_e^2}{12\pi^2} \left(\frac{M}{M_{Pl}} \right)^4 \frac{w^3(\chi_c)}{[w'(\chi_c)]^2}, \quad (13)$$

and the spectral index n_s , the ratio of tensor to scalar perturbations r and the running of n_s with the wavevector $dn_s/d \ln k$ become

$$n_s = 1 - 6 \epsilon_v + 2 \eta_v \quad , \quad r = 16 \epsilon_v \quad (14)$$

$$\frac{dn_s}{d \ln k} = -\frac{2}{N_e^2} \left\{ \frac{w'(\chi_c)w'''(\chi_c)}{w^2(\chi_c)} + 3 \left[\frac{w'(\chi_c)}{w(\chi_c)} \right]^4 - 4 \frac{[w'(\chi_c)]^2 w''(\chi_c)}{w^3(\chi_c)} \right\}. \quad (15)$$

The virtue of the $1/N_e$ expansion is that we can choose a reference baseline value for N_e , say $N_e = 50$ for numerical study, and use the scaling with N_e of the slow roll parameters given by eqs.(10), (14) and (15) to obtain their values for arbitrary N_e , namely

$$\epsilon_v[N_e] = \epsilon_v[50] \frac{50}{N_e} \quad , \quad \eta_v[N_e] = \eta_v[50] \frac{50}{N_e} \quad , \quad r[N_e] = r[50] \frac{50}{N_e} \quad ,$$

$$\frac{dn_s}{d \ln k}[N_e] = \frac{dn_s}{d \ln k}[50] \left(\frac{50}{N_e} \right)^2 \quad , \quad n_s[N_e] = n_s[50] + (1 - n_s[50]) \frac{N_e - 50}{N_e}. \quad (16)$$

In what follows we will take $N_e = 50$ as representative of the cosmologically relevant case, however, the simple scaling relations (16) allow a straightforward extrapolation to other values.

The combination of WMAP and SDSS (LRG) data yields [6]

$$n_s = 0.958 \pm 0.016 \quad (\text{assuming } r = 0 \text{ with no running}) \quad (17)$$

$$r < 0.28 \quad (95\% \text{ CL}) \quad \text{no running} \quad (18)$$

$$r < 0.67 \quad (95\% \text{ CL}) \quad \text{with running} \quad (19)$$

The running must be very small and of the order $\mathcal{O}(1/N_e^2) \sim 10^{-3}$ in slow roll for generic potentials[15]. Therefore, we can safely consider $dn_s/d \ln k = 0$ in our analysis. Figure 14 in ref.[6] and figure 2 in ref.[20] show that the preferred value of n_s slowly grows with the preferred value of r for $r > 0$. We find approximately that

$$\frac{\Delta n_s}{\Delta r} \simeq 0.12 \quad (20)$$

Therefore, for $r \sim 0.1$ the central value of n_s shifts from $n_s = 0.958$ ($r = 0$) to $n_s = 0.97$ ($r = 0.1$) as can be readily gleaned from the quoted figures in these references.

As a simple example that provides a guide post for comparison let us consider first the monomial potential

$$V(\phi) = \frac{\lambda}{2n} \phi^{2n}. \quad (21)$$

The case $n = 1$ yields a satisfactory fit to the WMAP data [5, 6]. For these potentials it follows that,

$$w(\chi) = \frac{\chi^{2n}}{2n} ; \quad M^4 = \lambda N_e^{n-1} M_{Pl}^{2n}, \quad (22)$$

inflation ends at $\chi_{end} = 0$, and the value of the dimensionless field χ_c at N_e e-folds before the end of inflation is

$$|\chi_c| = 2 \sqrt{n}. \quad (23)$$

These results lead to [2]

$$\epsilon_v = \frac{n}{2N_e} , \quad \eta_v = \frac{2n-1}{2N_e} \quad (24)$$

$$n_s - 1 = -\frac{n+1}{N_e} , \quad r = \frac{8n}{N_e} , \quad \frac{dn_s}{d \ln k} = -\frac{n+1}{N_e^2}. \quad (25)$$

Taking $N_e = 50$ as a baseline, these yield

$$n_s - 1 = -2(n+1) \times 10^{-2} \left(\frac{50}{N_e}\right) , \quad r = 0.16n \left(\frac{50}{N_e}\right) , \quad \frac{dn_s}{d \ln k} = -4(n+1) \times 10^{-4} \left(\frac{50}{N_e}\right)^2. \quad (26)$$

III. FAMILY OF MODELS

We study the CMB observables $n_s, r, dn_s/d \ln k$ for families of new inflation and chaotic models determined by the following inflationary potentials.

$$V(\phi) = V_0 - \frac{1}{2} m^2 \phi^2 + \frac{\lambda}{2n} \phi^{2n} , \quad \text{broken symmetry} \quad (27)$$

$$V(\phi) = \frac{1}{2} m^2 \phi^2 + \frac{\lambda}{2n} \phi^{2n} , \quad \text{unbroken symmetry} . \quad (28)$$

Upon introducing the rescaled field χ given by eq. (7) we find that these potentials can be written as

$$V(\phi) = N_e m^2 M_{Pl}^2 w(\chi) , \quad (29)$$

where we recognize that

$$M^4 = m^2 M_{Pl}^2 . \quad (30)$$

Then, the family of potentials eqs.(27)-(28) are

$$w(\chi) = w_0 - \frac{1}{2} \chi^2 + \frac{g}{2n} \chi^{2n} , \quad \text{broken symmetry} \quad (31)$$

$$w(\chi) = \frac{1}{2} \chi^2 + \frac{g}{2n} \chi^{2n} , \quad \text{unbroken symmetry} . \quad (32)$$

where w_0 and g are dimensionless and related to V_0 and λ by

$$V_0 = w_0 N_e m^2 M_{Pl}^2 , \quad \lambda = \frac{m^2 g}{M_{Pl}^{2n-2} N_e^{n-1}} . \quad (33)$$

New inflation models described by the dimensionless potential given by eq. (31) feature a minimum at χ_0 which is the solution to the following conditions

$$w'(\chi_0) = w(\chi_0) = 0 . \quad (34)$$

These conditions yield,

$$g = \frac{1}{\chi_0^{2n-2}} \quad , \quad w_0 = \frac{\chi_0^2}{2n} (n-1) \quad , \quad (35)$$

χ_0 determines the scale of symmetry breaking ϕ_0 of the inflaton potential upon the rescaling eq.(7), namely

$$\phi_0 = \sqrt{N_e} M_{Pl} \chi_0 \quad . \quad (36)$$

It is convenient to introduce the dimensionless variable

$$x = \frac{\chi}{\chi_0} \quad (37)$$

Then, from eqs.(35) and (37), the family of inflation models eq.(31)-(32) take the form

$$w(\chi) = \frac{\chi_0^2}{2n} [n(1-x^2) + x^{2n} - 1] \quad , \quad \text{broken symmetry} \quad , \quad (38)$$

$$w(\chi) = \frac{\chi_0^2}{2n} [n x^2 + x^{2n}] \quad , \quad \text{unbroken symmetry} \quad . \quad (39)$$

In terms of the variable x , the small and large field regions for the potential eq.(38) correspond to $x < 1$ and $x > 1$, respectively. The form of the dimensionless potentials $w(x)$ for both families are depicted in fig. 1. The left panel in this figure shows the new (small field) or chaotic (large field) behavior of the broken symmetry potential eq.(38) depending on whether the initial value of the inflaton is smaller or larger than the minimum of the potential $x = 1$.

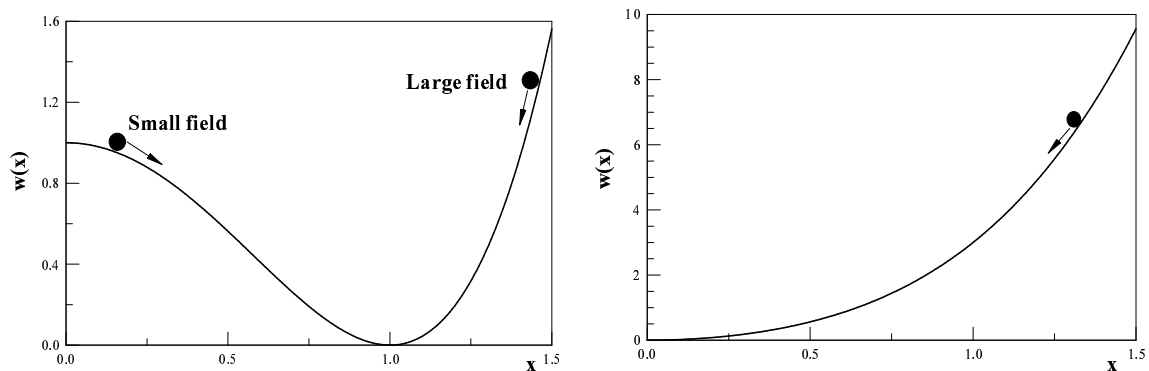


FIG. 1: Left panel: broken symmetry potential for $n = 2$, small and large field cases. Right panel: unbroken symmetry potential for $n = 2$, large field inflation.

IV. BROKEN SYMMETRY MODELS.

Inflation ends when the inflaton field arrives to the minimum of the potential. For the new inflation family of models eq.(38) inflation ends for

$$\chi_{end} = \chi_0 \quad . \quad (40)$$

In terms of the dimensionless variable x , the condition eq.(9) becomes

$$\frac{2n}{\chi_0^2} = I_n(X) \quad , \quad X = \frac{\chi_c}{\chi_0} \equiv x_c \quad , \quad (41)$$

where

$$I_n(X) = \int_X^1 \frac{dx}{x} \frac{n(1-x^2) + x^{2n} - 1}{1 - x^{2n-2}} = \int_X^1 \frac{n - \sum_{m=0}^{n-1} x^{2m}}{\sum_{m=0}^{n-2} x^{2m}} \frac{dx}{x} \quad . \quad (42)$$

This integral can be computed in closed form in terms of hypergeometric functions [23] which can be reduced to a finite sum of elementary functions[24].

For a fixed given value of X , the value of χ_0 and therefore of the dimensionless coupling g is determined by the equation (41). Once we obtain this value, the CMB observables eqs. (14)-(15) are obtained by evaluating the derivatives of $w(\chi)$ at the value $\chi = \chi_c = \chi_0 X$ with the corresponding value of the coupling g . Thus, a study of the range of possible values for n_s , r , $dn_s/d \ln k$ is carried out by exploring the relationship between these spectral indices as a function of X . For this study we choose the baseline value $N_e = 50$ from which the indices can be obtained for arbitrary value of N_e by the relation (16).

While the dependence of χ_0 and g upon the variable X must in general be studied numerically, their behavior in the relevant limits, $X \rightarrow (0, 1)$ for small field inflation and $X \gg 1$ for large field inflation can be derived from eqs.(41)-(42).

For small field inflation and $X \rightarrow 0$ the lower limit of the integral dominates leading to

$$\chi_0^2 \stackrel{X \rightarrow 0}{\cong} \frac{2n}{n-1} \frac{1}{\log \frac{1}{X}} \quad , \quad g \stackrel{X \rightarrow 0}{\cong} \left(\frac{n-1}{2n} \log \frac{1}{X} \right)^{n-1} \quad , \quad (43)$$

thus, as $X \rightarrow 0$ these are *strongly coupled theories*. This result has a clear and simple interpretation: for $N_e = 50$ to be the number of e-folds between $x = X$ and $x = 1$ the coupling g must be large and the potential must be steep, otherwise there would be many more e-folds in such interval.

For small field inflation and $X \rightarrow 1^-$ the integral $I_n(X)$ obviously vanishes and

$$\chi_0^2 \stackrel{X \rightarrow 1^-}{\cong} \left(\frac{2}{1-X} \right)^2 \left[1 + \frac{2n-1}{9} (X-1) + \mathcal{O}(X-1)^2 \right] \quad , \quad g \stackrel{X \rightarrow 1^-}{\cong} \left[\frac{1}{2} (1-X) \right]^{2(n-1)} \rightarrow 0 \quad , \quad (44)$$

thus, as $X \rightarrow 1^-$, these are a *weakly coupled family of models*.

For large field inflation and $X \gg 1$, the integral $I_n(X)$ is dominated by the term with the highest power, namely x^{2n} , leading to the behavior

$$\chi_0^2 \stackrel{X \gg 1}{\cong} \frac{4n}{X^2} \quad , \quad g \stackrel{X \gg 1}{\cong} \left(\frac{X^2}{4n} \right)^{n-1} \quad , \quad (45)$$

which leads to a strongly coupled regime. The results of a numerical analysis are depicted in fig. 2.

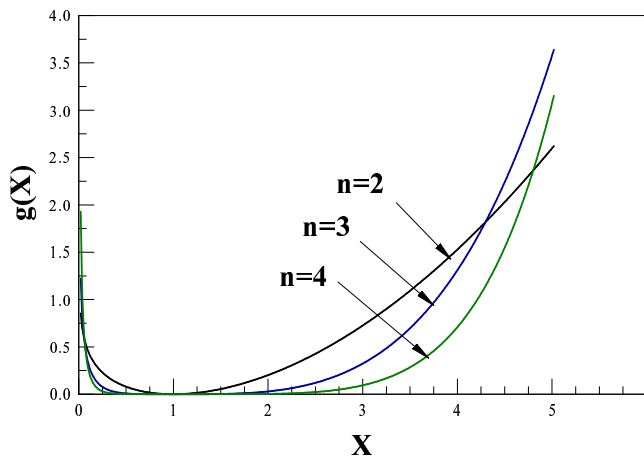


FIG. 2: The coupling g as a function of X , for the degrees of the new inflation potential $n = 2, 3, 4$. For $X \rightarrow 1$, g vanishes as $\left[\frac{1-X}{2} \right]^{2(n-1)}$. The point $X = 1, g = 0$ corresponds to the monomial $m^2 \phi^2/2$. g increases both for $X \rightarrow 0$ and for large X as, $\left(\log \frac{1}{X} \right)^{n-1}$ and $\left(\frac{X^2}{4n} \right)^{n-1}$, respectively.

Before we proceed with a numerical study of the CMB indices and the tensor to scalar ratio, we can extract interesting and relevant information by focusing on the region $X \sim 1$ which as discussed above corresponds to a

weakly coupled family for broken symmetry potentials. This is the region near the *minimum* of the potential and the integral $I_n(X)$ can be evaluated simply by expanding $w(\chi)$ and its derivative near the minimum. To leading order in $(X - 1)$ the condition (41) leads to eq.(44) and

$$(\chi_c - \chi_0)^2 = 4 \quad \text{or} \quad |\chi_c - \chi_0| = 2. \quad (46)$$

This is precisely eq.(23) for $n = 1$ upon the shift $\chi_c \rightarrow \chi_c - \chi_0$. Namely, eq.(46) is the condition eq.(23) for the quadratic monomial potential with minimum at $\chi = \chi_0$ instead of $\chi = 0$ as in eq.(22). This is clearly a consequence of the fact that near the minimum $X = 1$ the potential is quadratic, therefore for $X \sim 1$ the quadratic monomial is an excellent approximation to the family of higher degree potentials and more so because $g \sim 0$. For $X \sim 1$ we find to leading order in $(X - 1)$ the values:

$$\epsilon_v = \eta_v = 0.01 \left(\frac{50}{N_e} \right), \quad n_s = 0.96 + 0.04 \left(\frac{N_e - 50}{N_e} \right), \quad r = 0.16 \left(\frac{50}{N_e} \right), \quad \frac{dn_s}{d \ln k} = -0.0008 \left(\frac{50}{N_e} \right)^2. \quad (47)$$

The fact that the potential eq.(38) is quadratic around the minimum $X = 1$ explains why we have in this limit identical results for new inflation with the potential eq.(38) and chaotic inflation with the monomial potential $m^2 \phi^2/2$.

As observed in [6] these values of r , n_s for $N_e \sim 50$ yield a good fit to the available CMB data.

The results of the numerical analysis for ϵ_v , η_v , n_s , r and $dn_s/d \ln k$ for the baseline value $N_e = 50$ are depicted in fig. 3, 4, 5 and 6 respectively.

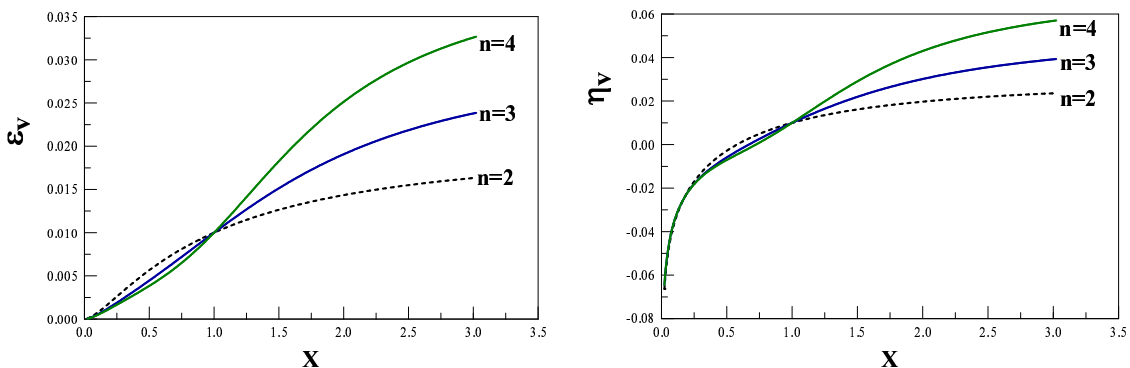


FIG. 3: Slow roll parameters as a function of X for $N_e = 50$. Left panel ϵ_v , right panel η_v , for new inflation with the degrees of the potential $n = 2, 3, 4$. The results for arbitrary values of N_e are obtained by multiplying by the factor $\frac{50}{N_e}$.

The vertical dashed line in fig. 4 at $X \sim 0.2$ determines the lower limit of X for which n_s is consistent with the WMAP data for $r = 0$. For large values of X , n_s approaches asymptotically the values for the monomial potentials ϕ^{2n} given by eq. (26). For the larger degrees n , the asymptotic behavior of n_s and r settles at larger values of X , this is a consequence of the larger region in which the coupling is small as observed in fig. 2 for larger degrees n . The horizontal dashed lines with vertical downward arrows in fig. 5 determines the upper bound from WMAP [6] given by eq. (19) *without* running, since from fig. 6 the values of $dn_s/d \ln k$ for these models are negligible. The vertical dashed line with the right-pointing arrow in fig. 5 determines the values of X for which n_s are consistent with the WMAP data (see also fig. 4).

From these figures we see that unlike the case of a pure monomial potential $\lambda \phi^{2n}$ with $n \geq 2$, there is a **large** region of field space within which the new inflation models given by eq.(27) are **consistent** with the bounds from marginalized WMAP3 data and the combined WMAP3 + LSS data [6].

Fig. 7 displays r vs n_s for the values $n = 2, 3, 4$ in new inflation and indicate the trend with n . While r is a monotonically increasing function of X , n_s features a *maximum* as a function of X , hence r becomes a **double-valued** function of n_s . The grey dot at $r = 0.16$, $n_s = 0.96$ corresponds to the monomial potential $m^2 \phi^2/2$ for $N_e = 50$. Values below the grey dot along the curve in fig. 7 correspond to small fields $X < 1$ while values above it correspond to large fields $X > 1$. We see from figs. 5 and 7 that *large fields systematically lead to larger values of r* . Models that fit the WMAP data to 95% *CL* are within the tilted box in fig. 7. The tilt accounts for the growth of the preferred value of n_s with r [6] according to eq. (20).

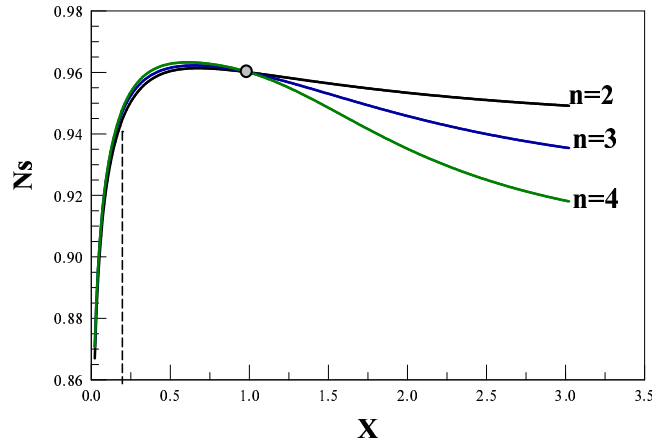


FIG. 4: Scalar spectral index n_s for the degrees of the potential $n = 2, 3, 4$ for new inflation with $N_e = 50$. The vertical line delimits the smallest value of n_s (for $r = 0$) [6]. The grey dot at $n_s = 0.96$, $X = 1$ corresponds to the value for the monomial potential $n = 1$, $m^2 \phi^2/2$. Notice that the small field behavior is n independent. For arbitrary N_e the result follows directly from the $N_e = 50$ value by using eq.(16).

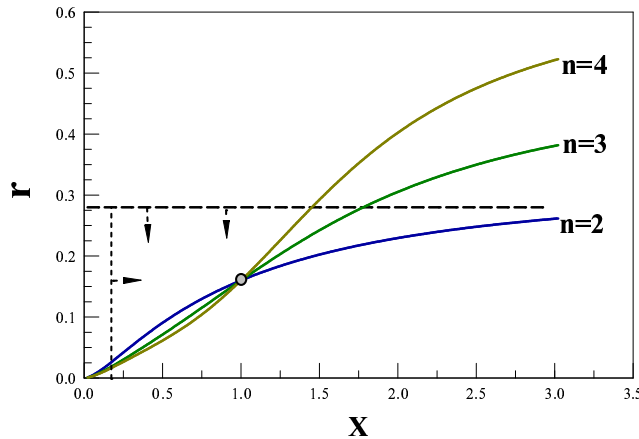


FIG. 5: Tensor to scalar ratio r vs. X for the degrees of the potential $n = 2, 3, 4$ for new inflation with $N_e = 50$. The horizontal dashed line corresponds to the upper limit $r = 0.28$ (95%CL) from WMAP3 without running. The vertical dashed line determines the minimum value of X , $X \sim 0.2$, consistent with the WMAP limits for n_s as in fig. 4. The grey dot at $X = 1$, $r = 0.16$ corresponds to the value for the monomial potential $m^2 \phi^2/2$. The small field limit is nearly independent of n . For arbitrary N_e the result follows directly from the $N_e = 50$ value by using eq. (16).

Fig. 8 displays the running of the scalar index vs. n_s for the different members of the family of new inflation showing clearly that running is all but negligible in the entire range of values consistent with the WMAP data. This was expected since the running in slow-roll is of the order $\sim \frac{1}{N_e^2} \simeq 4 \times 10^{-4}$ [see eq.(15)] [15].

We note that $dn_s/d \ln k$ is a monotonically *decreasing* function of X approaching asymptotically the values for the monomials ϕ^{2n} given by eq. (26). $X \sim 0.2$ which is the *minimum value* of X consistent with the bounds from WMAP on n_s (see fig. 4).

A. Field reconstruction

The above analysis suggests to study the *inverse problem*, namely, for a given member of the family labeled by n , we may ask what is the value ϕ_c of the field at Hubble crossing and what is the scale ϕ_0 of symmetry breaking of

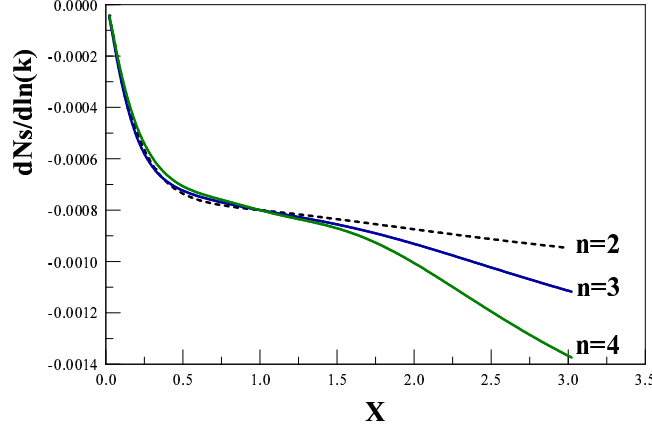


FIG. 6: Running of the scalar index $dn_s/d\ln k$ vs. X for the degrees of the potential $n = 2, 3, 4$ respectively for new inflation with $N_e = 50$. The small field behavior is independent of n . For arbitrary N_e the result follows directly from the $N_e = 50$ value by using eq. (16).

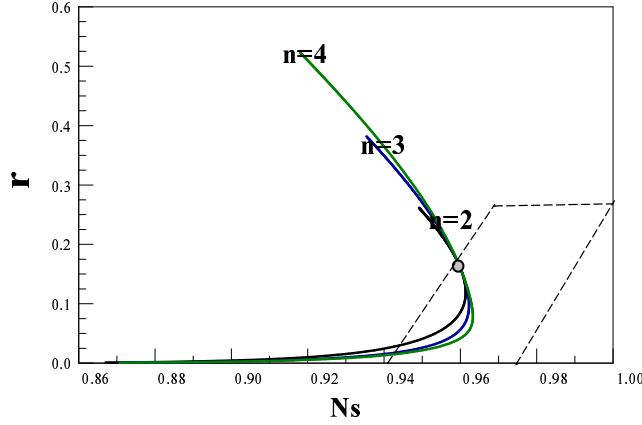


FIG. 7: Tensor to scalar ratio r vs. n_s for degrees of the potential $n = 2, 3, 4$ respectively for new inflation with $N_e = 50$. r turns to be a **double-valued** function of n_s exhibiting a maximum value for n_s . The values inside the box between the dashed lines correspond to the WMAP3 marginalized region of the (n_s, r) plane with (95%CL) : $r < 0.28$, $0.942 + 0.12 r \leq n_s \leq 0.974 + 0.12 r$, see eq.(20). The grey dot corresponds to the values for the monomial potential $m^2\phi^2/2$ and the value $X = 1$: $r = 0.16$, $n_s = 0.96$.

the potential which are consistent with the CMB+LSS data. This is tantamount to the program of reconstruction of the inflaton potential advocated in ref. [16] and is achieved as follows: eq.(41) yields $\chi_0 = \chi_0[X]$ from which we obtain $\chi_c = \chi_0 X$. These results are then input into the expression for n_s by evaluating the potential $w(\chi)$ and its derivatives at the value of χ_c . This yields $n_s = n_s[\chi_c]$ which is then inverted to obtain $\chi_c = \chi_c[n_s]$ and thus ϕ_c .

In the region $X \sim 1$ corresponding to the weakly coupled case, this reconstruction program can be carried out as a systematic series in

$$\Delta \equiv X - 1 = \frac{\chi_c}{\chi_0} - 1, \quad (48)$$

by expanding the inflationary potential and its derivatives in a power series in x around $x = 1$ in the integrand of $I_n(X)$ [eq. (42)]. For $X = 1$ the value of the scalar index n_s is determined by the simple monomial $m^2\phi^2/2$ from eq. (25) for $n = 1$ is given by $n_s - 1 = -2/N_e$. Therefore, in terms of n_s , the actual expansion parameter is $n_s - 1 + 2/N_e$.

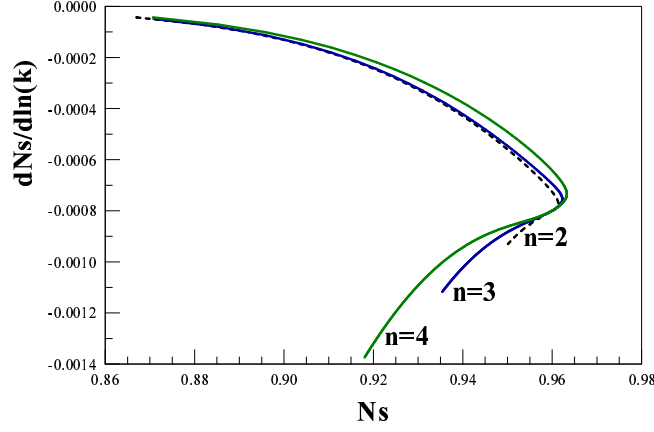


FIG. 8: Running of the scalar index $dn_s/d\ln k$ vs. n_s for degrees of the potential $n = 2, 3, 4$ respectively for new inflation with $N_e = 50$. The values for arbitrary N_e follow directly from the $N_e = 50$ value by using eq. (16).

We obtain n_s to first order in Δ from eqs.(10), (14), (38), (44) and (48) with the result,

$$n_s - 1 = -\frac{2}{N_e} \left[1 + \frac{2n-1}{18} \Delta + \mathcal{O}(\Delta^2) \right]$$

then, by inverting this equation we find:

$$\Delta(n_s, n) = X - 1 = -\frac{9N_e}{2n-1} \left(n_s - 1 + \frac{2}{N_e} \right) + \mathcal{O} \left(\left[n_s - 1 + \frac{2}{N_e} \right]^2 \right), \quad (49)$$

and from eqs. (44) and (49) we find,

$$\chi_0(n_s, n) = \frac{2(2n-1)}{9N_e \left| n_s - 1 + \frac{2}{N_e} \right|} \left[1 - \frac{N_e}{2} \left(n_s - 1 + \frac{2}{N_e} \right) \right] + \mathcal{O} \left(\left[n_s - 1 + \frac{2}{N_e} \right] \right) \quad (50)$$

The leading order ($\propto 1/\Delta$) of this result for $\chi_0(n_s, n)$ can be simply cast as eq.(46): this is recognized as the condition to have 50 e-folds for the quadratic monomial centered in the broken symmetry minimum [see discussion below eq. (46)].

Finally, the value of the (dimensionless) field χ_c at Hubble crossing is determined from $\chi_c(n_s, n) = \chi_0 [1 + \Delta(n_s, n)]$ from which we obtain

$$\chi_c = \frac{2(2n-1)}{9N_e \left| n_s - 1 + \frac{2}{N_e} \right|} \left[1 - \frac{(2n+17)N_e}{2(2n-1)} \left(n_s - 1 + \frac{2}{N_e} \right) \right] + \mathcal{O} \left(\left[n_s - 1 + \frac{2}{N_e} \right] \right). \quad (51)$$

The coupling constant g can be also expressed in terms of n_s in this regime with the result,

$$g = \left[\frac{9N_e \left| n_s - 1 + \frac{2}{N_e} \right|}{2(2n-1)} \right]^{2n-2} \rightarrow 0,$$

which exhibits the weak coupling character of this limit.

This analysis shows that the region in field space that corresponds to the region in n_s that *best fits the WMAP data* can be systematically reconstructed in an expansion in $n_s - 1 + 2/N_e$. This is yet another bonus of the $1/N_e$ expansion. Although the above analysis can be carried out to an arbitrary order in $n_s - 1 + 2/N_e$, it is more convenient to perform a numerical study of the region outside from $X \sim 1$ to find the values of χ_c and χ_0 as a function of n_s for fixed values of n , N_e . Figures 9 and 10 display χ_c , χ_0 as a function of n_s with $N_e = 50$ for different values of n for the small field region $X < 1$ and the large field region $X > 1$ respectively. The point $X = 1$ is a degeneracy point and corresponds to the quadratic monomial as discussed above.

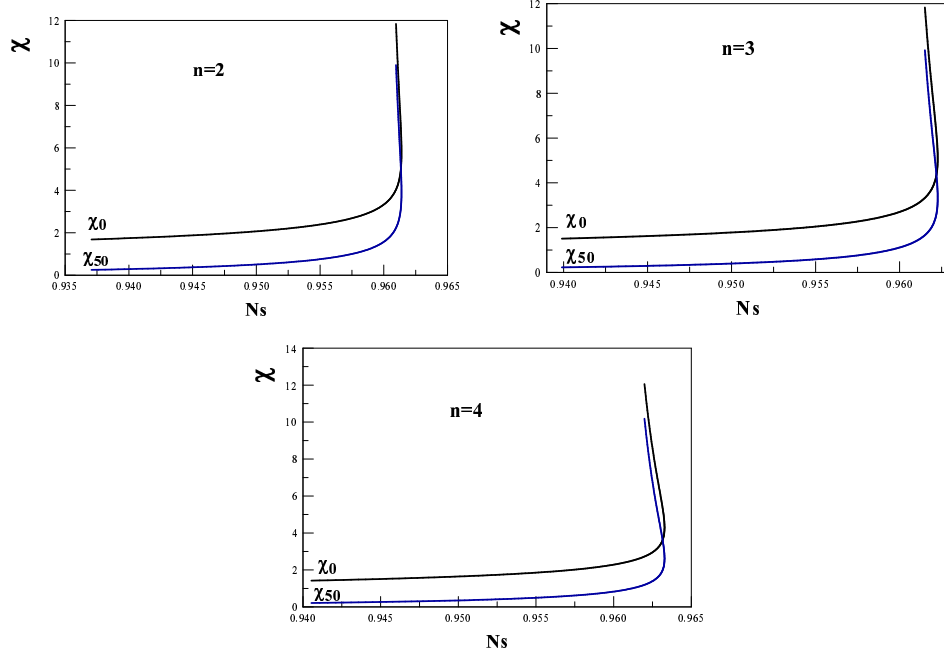


FIG. 9: Reconstruction program for broken symmetry potentials with $N_e = 50$, small field case $X < 1$. $\chi_{50} \equiv \chi_c$ and χ_0 vs. n_s for degrees of the potential $n = 2, 3, 4$, respectively. These values of χ_c , n_s correspond to the region $r < 0.16$.

Finally, the values for the dimensionful field ϕ are given by $\phi_c = \sqrt{N_e} M_{Pl} \chi_c$, $\phi_0 = \sqrt{N_e} M_{Pl} \chi_0$. Figures 7, 9 and 10 lead to the conclusion that for the range of CMB parameters $r < 0.1$ and $n_s \leq 0.96$, the typical value of the *symmetry breaking scale* is $\phi_0 \sim 10 M_{Pl}$ and the value of the inflaton field at which cosmologically relevant wavelengths crossed the Hubble radius during new inflation is $\phi_c \sim M_{Pl}$ with a weak dependence on n . For $0.1 < r < 0.16$ we have $|\phi_c - \phi_0| \sim 15 M_{Pl}$.

We obtain for the coupling g in the $X \rightarrow 0$ limit which is a strong coupling regime [see eq.(43)] where $n_s \ll 1$,

$$g = \left[\frac{N_e}{4} \left(1 - \frac{1}{n} \right) (1 - n_s) \right]^{n-1}.$$

Finally, we have the $X \rightarrow \infty$ limit which is also a strong coupling limit [see eq.(45)] where $n_s \rightarrow 1 - (n+1)/N_e$ and we find,

$$\begin{aligned} \chi_0^2 &= (4n)^2 \left[\frac{N_e(1 - n_s) - (n+1)}{4n(n-1) + 3 \left(1 + \frac{1}{n-2} \right)} \right]^{\frac{1}{n-1}} \rightarrow 0 \\ g &= \frac{4n(n-1) + 3 \left(1 + \frac{1}{n-2} \right)}{(4n)^{n-1} [N_e(1 - n_s) - (n+1)]} \rightarrow \infty. \end{aligned} \quad (52)$$

V. CHAOTIC INFLATION MODELS.

We now turn to the study of the family of chaotic inflationary potentials given by eq. (39). Taking that the end of inflation corresponds to $x = 0$, the condition eq.(9) now becomes

$$\frac{2n}{\chi_0^2} = J_n(X) = \int_0^X \frac{n + x^{2n-2}}{1 + x^{2n-2}} x dx. \quad (53)$$

Again, this integral can be computed in closed form in terms of hypergeometric functions [23] which can be reduced to a finite sum of elementary functions[24]. For general values of X the integral will be studied numerically, but the

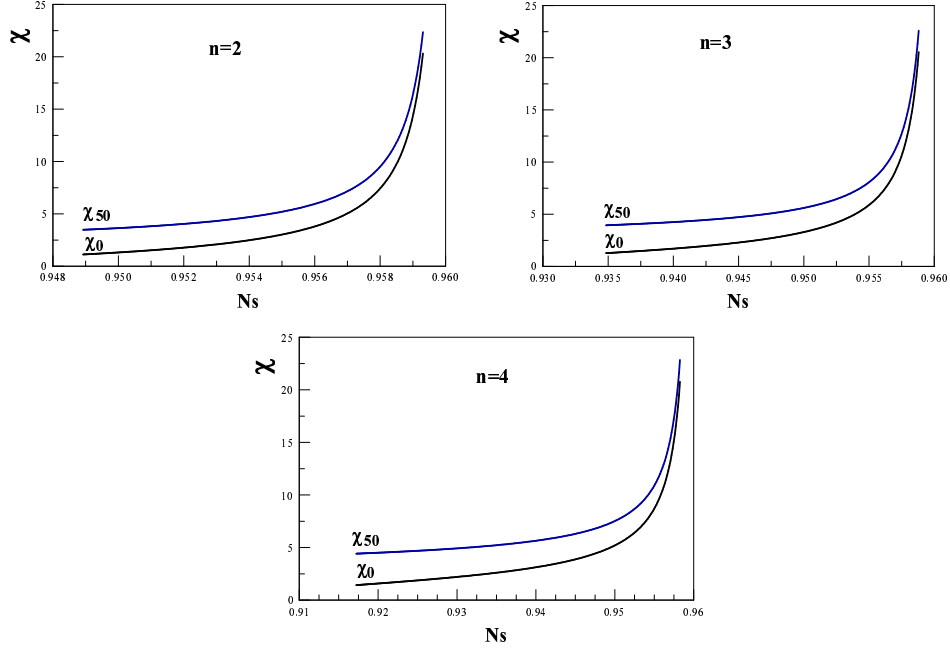


FIG. 10: Reconstruction Program for broken symmetry potentials with $N_e = 50$, large field case $X > 1$. $\chi_{50} \equiv \chi_c$ and χ_0 vs. n_s for degrees of the potential $n = 2, 3, 4$, respectively. These values of χ , n_s correspond to the region $r > 0.16$.

small X region can be studied by expanding the integrand in powers of x^{2n-2} , with the result

$$1 = \frac{\chi_0^2 X^2}{4} \left[1 - \frac{n-1}{n^2} X^{2n-2} + \mathcal{O}(X^{4n-4}) \right]. \quad (54)$$

For small X and recalling that $X = \chi_c/\chi_0$ this relation yields

$$|\chi_c| = 2 \left[1 + \frac{n-1}{2n^2} X^{2n-2} + \mathcal{O}(X^{4n-4}) \right] \quad (55)$$

which is again, at dominant order the relation for the quadratic monomial potential eq.(23) for $n = 1$. This must be the case because the small field limit is dominated by the quadratic term in the potential. For small fields, $\chi_0 \approx 2/X$ and the coupling g vanishes as,

$$g(X) \stackrel{X \rightarrow 0}{\approx} \left(\frac{X}{2} \right)^{2n-2}. \quad (56)$$

The coupling as a function of X is shown in fig. 11.

The dependence of ϵ_v , η_v in the full range of X for several representative values of n is studied numerically: these results are displayed in fig. 12. In the small X regime, we obtain from eqs. (10), (39) and (54) the expressions,

$$\epsilon_v = \frac{1}{2N_e} \left[1 + \frac{(2n-1)(n-1)}{n^2} X^{2n-2} + \mathcal{O}(X^{4n-4}) \right] \quad (57)$$

$$\eta_v = \frac{1}{2N_e} \left[1 + \frac{(2n-1)(n^2-1)}{n^2} X^{2n-2} + \mathcal{O}(X^{4n-4}) \right] \quad (58)$$

As $X \rightarrow 0$, ϵ_v and η_v tend to the result from the quadratic monomial potential, namely $\epsilon_v = \eta_v = 1/[2N_e]$ as must be the case because the quadratic term dominates the potential for $X \ll 1$.

Figures 13, 14 display n_s , r as functions of X for $N_e = 50$ respectively. For $X \rightarrow 0$, $n_s \rightarrow 0.96$ and $r \rightarrow 0.16$ which are the values from the quadratic monomial $m^2 \phi^2/2$.

For $X \gg 1$, the values of n_s , r for the monomial potentials ϕ^{2n} are attained asymptotically, namely, (for $N_e = 50$): $n_s - 1 = -2(n+1) \times 10^{-2}$, $r = 0.16n$.

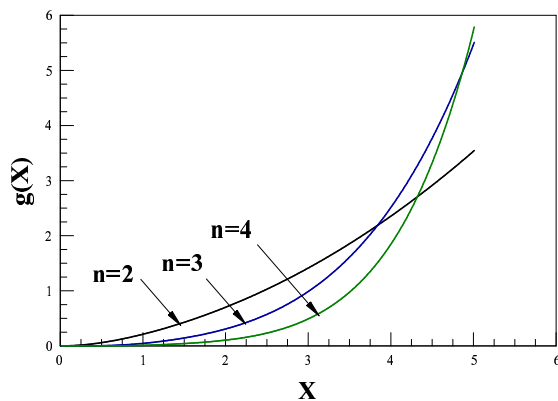


FIG. 11: Coupling g as a function of X for $N_e = 50$, for $n = 2, 3, 4$ for chaotic inflation. g turns to be a monotonically increasing function of X . g vanishes for $X \rightarrow 0$ as $(\frac{X}{2})^{2n-2}$ in sharp contrast with new inflation where g strongly increases for $X \rightarrow 0$.

Comparing figs. 13, 14 to those for the new inflation case, (figs. 4 and 5), we note that the range in which the chaotic family provide a good fit to the WMAP data is *very much smaller* than for new inflation. Fig. 13 shows that in chaotic inflation *only* for $n = 2$ the range of n_s is allowed by the WMAP data in a fairly extensive range of values of X , whereas for $n = 3, 4$ (and certainly larger), there is a *relatively small* window in field space for $X < 1$ which satisfies the data for n_s and r simultaneously.

The tensor to scalar ratio r in chaotic inflationary models is *larger* than 0.16 for all values of X , approaching asymptotically for large X the value $r = 0.16n$ associated to the monomial potentials ϕ^{2n} .

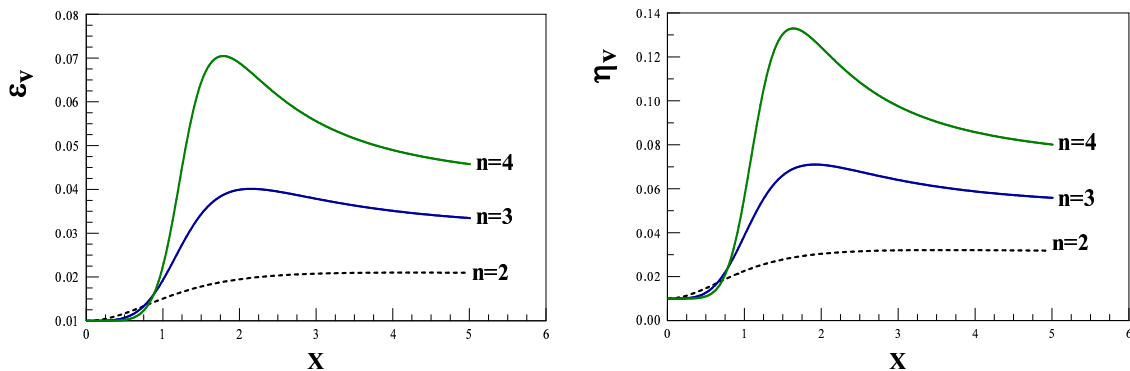


FIG. 12: Left panel ϵ_v , right panel η_v as a function of X for $N_e = 50$, for chaotic inflation with degrees of the potential $n = 2, 3, 4$. The small X behavior is n independent.

Fig. 15 displays $dn_s/d \ln k$ as a function of X , while the running is again negligible, it is *strikingly different* from the new inflation case. *Again* this figure, in combination with those for n_s and r as functions of X distinctly shows that **only** $n = 2$ in chaotic inflation is compatible with the bounds from the WMAP data, while for $n = 3, 4$ only a *small window* for $X < 1$ is allowed by the data. We see from fig. 15 that $dn_s/d \ln k$ takes negative as well as positive values for chaotic inflation, in contrast with new inflation where $dn_s/d \ln k < 0$.

The fact that the combined bounds on n_s , r and $dn_s/d \ln k$ from the WMAP3 data [6] provide much more stringent constraints on chaotic models is best captured by displaying r as a function of n_s in fig. 16. The region allowed by the WMAP data lies within the tilted box delimited by the vertical and horizontal dashed lines that represent the 95%CL band [6].

A complementary assessment of the allowed region for this family of effective field theories is shown in fig. 17 which distinctly shows that **only** the $n = 2$ case of chaotic inflation is allowed by the WMAP3 data.

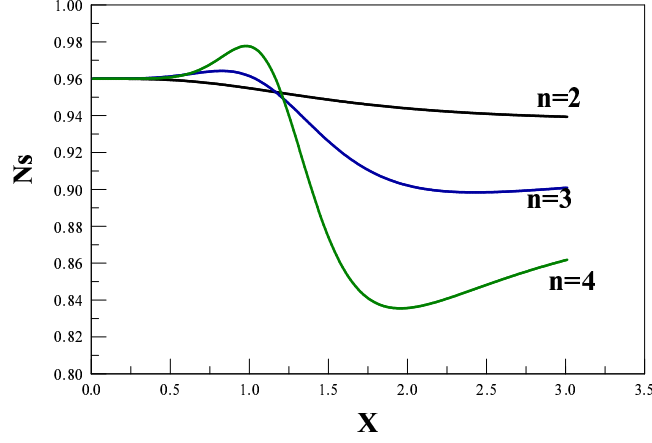


FIG. 13: Scalar spectral index n_s for degrees of the potential $n = 2, 3, 4$ respectively for chaotic inflation with $N_e = 50$. For $X \rightarrow 0$, n_s reaches for all n the value $n_s = 0.96$ corresponding to the monomial potential $m^2\phi^2/2$.

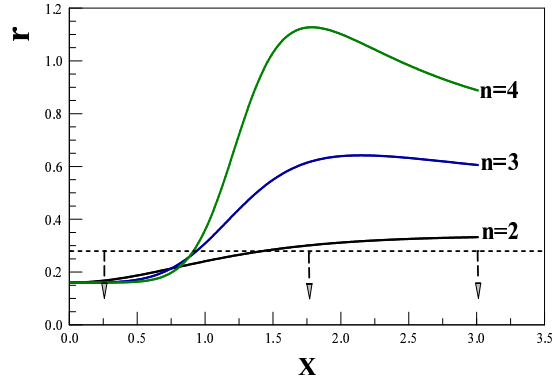


FIG. 14: Tensor to scalar ratio r vs. X for degrees of the potential $n = 2, 3, 4$ respectively for chaotic inflation with $N_e = 50$. The horizontal dashed lines with the downward arrows delimit the region of 95% CL given by WMAP3 with no running $r < 0.28$ [6].

A. Field reconstruction

The reconstruction program proceeds in the same manner as in the case of new inflation: the first step is to obtain $\chi_0(X)$ from eq.(53). Then ϵ_v and η_v are obtained as a function of X which yields $n_s(X)$. Inverting this relation we find $X = X(n_s)$ and finally $\chi_c(n_s) = \chi_0(X(n_s))$. While this program must be carried out numerically, we can gain important insight by focusing on the small X region and using eq.(54).

From eqs. (14), (57) and (58) we find

$$n_s - 1 + \frac{2}{N_e} = X^{2n-2} \frac{(2n-1)(n-1)(n-2)}{n^2 N_e} + \mathcal{O}(X^{4n-4}) \quad (59)$$

As $X \rightarrow 0$ it follows that $n_s \rightarrow 1 - 2/N_e$ which is the value for the scalar index for the quadratic monomial potential $m^2\phi^2/2$. However, for $n > 2$ this limit is approached from above, namely for $n > 2$ it follows that $n_s > 1 - 2/N_e$. The small X region corresponds to small departures of n_s from the value determined by the quadratic monomial $1 - 2/N_e$ but always larger than this value for $n > 2$. In the small field limit we reconstruct the value of χ_c in an expansion in $n_s - 1 + 2/N_e$. The leading order in this expansion is obtained by combining eqs. (55) and (59), we obtain

$$|\chi_c| = 2 \left[1 + \frac{(n_s - 1 + \frac{2}{N_e})N_e}{2(2n-1)(n-2)} \right] + \mathcal{O}([n_s - 1 + 2/N_e]^2) \quad (60)$$

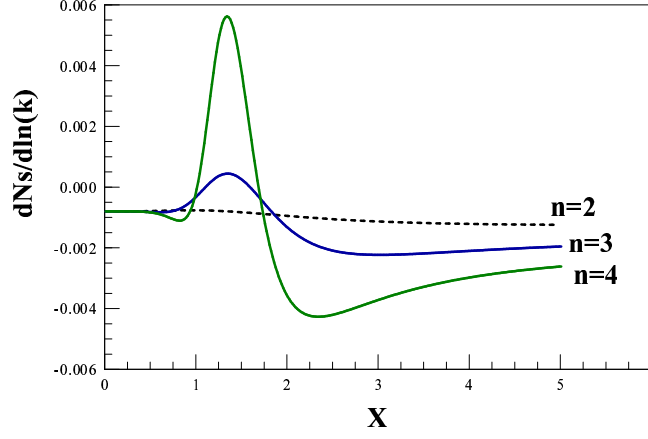


FIG. 15: Running of the scalar index $dn_s/d \ln k$ vs. X for degrees of the potential $n = 2, 3, 4$ respectively for chaotic inflation with $N_e = 50$. The $X \rightarrow 0$ behavior is n independent. $dn_s/d \ln k$ features a maximum value that gets stronger with increasing n . For chaotic inflation $dn_s/d \ln k$ takes negative as well as positive values, in contrast with new inflation where $dn_s/d \ln k < 0$.

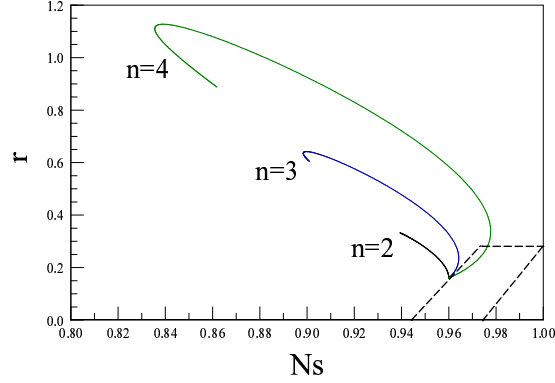


FIG. 16: Tensor to scalar ratio r vs. n_s for degrees of the potential $n = 2, 3, 4$ respectively for chaotic inflation with $N_e = 50$. The range of 95% CL as determined by WMAP3 [6] is within the tilted box delimited by : $r < 0.28$, $0.942 + 0.12 r \leq n_s \leq 0.974 + 0.12 r$, see eq.(20).

Obviously, this leading order term is singular at $n = 2$, this is a consequence of the result eq.(59) which entails that for $n = 2$ the expansion must be pursued to higher order, up to X^{4n-4} .

We find from eqs. (14), (57) and (58) for $n = 2$,

$$n_s - 1 + \frac{2}{N_e} = -\frac{17}{24 N_e} X^4 + \mathcal{O}(X^6) \quad , \quad n = 2, \quad (61)$$

therefore,

$$|\chi_c| = 2 \left[1 + \sqrt{\frac{3 N_e}{136} \left(1 - \frac{2}{N_e} - n_s \right)} \right] + \mathcal{O} \left(n_s - 1 + \frac{2}{N_e} \right) \quad , \quad n = 2. \quad (62)$$

We see that the derivative of χ_c with respect to n_s is singular for $n = 2$ at $n_s = 1 - \frac{2}{N_e}$. We note that for $n = 2$ there is a sign change with respect to the cases $n > 2$ and $n_s - 1 + 2/N_e \leq 0$ as determined by eq. (61).

Fig. 18 shows χ_c as a function of n_s for $n = 2, 3, 4$ for $N_e = 50$. The case $n = 2$ clearly shows the singularity in the derivative $\partial \chi_c / \partial n_s$ at $n_s = 1 - 2/N_e = 0.96$ [see eq.(62)].

Combining fig. 18 with fig. 16 it is clear that there is a small window in field space within which chaotic models

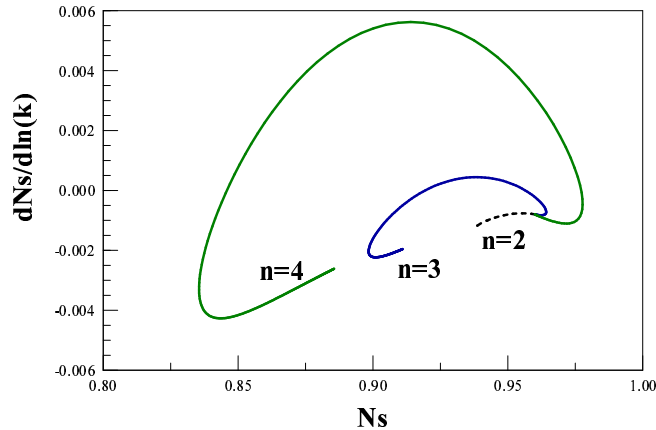


FIG. 17: Running of the scalar index $dn_s/d \ln k$ vs. n_s for degrees of the potential $n = 2, 3, 4$ respectively for chaotic inflation with $N_e = 50$.

provide a good fit to the WMAP3 data, for $N_e = 50$ we find:

$$\begin{aligned}
 n = 2 & : 0.95 \lesssim n_s \leq 0.960, \quad 2.0 \leq |\chi_c| \lesssim 2.25 \\
 n = 3 & : 0.96 \leq n_s \lesssim 0.965, \quad 2.0 \leq |\chi_c| \lesssim 2.15 \\
 n = 4 & : 0.96 \leq n_s \leq 0.975, \quad 2.0 \leq |\chi_c| \lesssim 2.10.
 \end{aligned} \tag{63}$$

Restoring the dimensions via eq. (7) these values translate into a narrow region of width $\Delta\phi \lesssim 1.5 M_{Pl}$ around the scale $|\phi_c| \sim 15 M_{Pl}$.

Therefore, the joint analysis for n_s , r , $dn_s/d \ln k$ distinctly reveals that: (i) chaotic models favor *larger* values of r thus, larger tensor amplitudes, and (ii) chaotic models feature *smaller* regions in field space consistent with the CMB and large scale structure data. *Only* the case $n = 2$ features a larger region of consistency with the combined WMAP3 data.

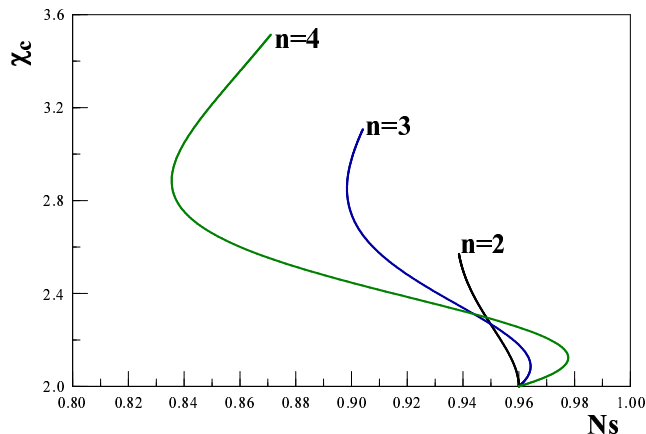


FIG. 18: Reconstruction program for chaotic inflation with $N_e = 50$, χ_c vs. n_s for $n = 2, 3, 4$ respectively.

VI. CONCLUSIONS

The fact that current observations of the CMB and LSS are already placing constraints on inflationary models which will undoubtedly become more stringent with forthcoming observations, motivates a study of the predictions

for the CMB power spectra from different inflationary scenarios. We perform a systematic study of *families* of single field new and chaotic inflation slow roll models characterized by effective field theories with potentials of the form

$$V(\phi) = V_0 - \frac{1}{2} m^2 \phi^2 + \frac{\lambda}{2n} \phi^{2n} \quad , \quad \text{broken symmetry} \quad (64)$$

$$V(\phi) = \frac{1}{2} m^2 \phi^2 + \frac{\lambda}{2n} \phi^{2n} \quad , \quad \text{unbroken symmetry} . \quad (65)$$

Unlike the approach followed in [5, 6] based on the inflationary flow equations[11], or more recent studies which focused on specific inflationary models [12], or on statistical analysis of models [13], we implement an expansion in $1/N_e$ where $N_e \sim 50$ is the number of e-folds before the end of inflation when wavelengths of cosmological relevance today cross the Hubble radius during inflation. We provide an analysis of the dependence of CMB observables (n_s , r and $dn_s/d \ln k$) with n and establish the region in field space within which these families provide a good agreement with the WMAP3 data combined with large scale surveys.

For new inflation models with potentials eq.(64) there are two distinct regions corresponding to values of the inflaton field smaller (small field) or larger (large field) than the symmetry breaking scale. For this family we find a **wide range** in the (n_s, r) plane in which the different members $n = 2, 3, 4 \dots$ are allowed by the data both for small and large fields with negligible running of the scalar index:

$$-4(n+1) \times 10^{-4} \leq dn_s/d \ln k \leq -2 \times 10^{-4} .$$

For $N_e = 50$ the values $n_s = 0.96, r = 0.16$ which are those determined by the simple monomial potential $m^2 \phi^2/2$ determine a divide and a degeneracy point in the field and parameter space. Small field regions yield $r < 0.16$ while large field regions correspond to $r > 0.16$.

The $1/N_e$ expansion also provides a powerful tool to implement a *reconstruction program* that allows to extract the value of the field N_e e-folds before the end of inflation, and in the case of new inflationary models, the symmetry breaking scale.

We find that the region of field space favored by the WMAP3 data can be explored in a systematic expansion in $n_s - 1 + 2/N_e$. An analytic and numerical study of this region lead us to conclude that if forthcoming data on tensor modes favors $r < 0.16$ then new inflation **is favored**, and we **predict** for $r < 0.1$ that (i) the **symmetry breaking scale** is

$$\phi_0 \sim 10 M_{Pl} ,$$

and (ii) the value of the field when cosmologically relevant wavelengths cross the Hubble radius is $|\phi_c| \sim M_{Pl}$.

The family of chaotic inflationary models characterized by the potentials eq.(65) feature tensor to scalar ratios $r \geq 0.16$ (for $N_e = 50$), with the minimum, $r = 0.16$ obtained in the limit of small inflaton amplitude and corresponds to the monomial potential $m^2 \phi^2/2$ which is again a degeneracy point for this family of models.

The combined marginalized data from WMAP3 [6] yields a very small window within which chaotic models are allowed by the data, the largest region of overlap with the (r, n_s) WMAP3 data corresponds to $n = 2$ and the width of the region decreases with larger n . The typical scale of the field at Hubble crossing for these models is $|\phi_c| \sim 15 M_{Pl}$ (for $N_e = 50$). Some small regions in field space consistent with the WMAP3 data feature peaks in the running of the scalar index but in the region consistent with the WMAP3 data in chaotic inflation the running is again negligible. If future observations determine a tensor to scalar ratio $r < 0.16$, such bound will, all by itself, **rule out** the large family of chaotic inflationary models of the form (65) for any n .

Acknowledgments

D. B. and C. M. Ho thank the US NSF for support under grant PHY-0242134, LPTHE and the Observatoire de Paris and LERMA for hospitality during this work. D.B. thanks A. Kosowsky for illuminating conversations.

-
- [1] D. Kazanas, *Astrophys. J* **241**, L59 (1980). A. Guth, *Phys. Rev.* **D23**, 347 (1981); astro-ph/0404546 (2004). K. Sato, *Mon. Not. R. Astron. Soc.* **195**, 467 (1981).
[2] E. W. Kolb and M. S. Turner, *The Early Universe* Addison Wesley, Redwood City, C.A. 1990. P. Coles and F. Lucchin, *Cosmology*, John Wiley, Chichester, 1995. A. R. Liddle and D. H. Lyth, *Cosmological Inflation and Large Scale Structure*, Cambridge University Press, 2000. S. Dodelson, *Modern Cosmology*, Academic Press, 2003. D. H. Lyth , A. Riotto, *Phys. Rept.* **314**, 1 (1999).

- [3] V. F. Mukhanov , G. V. Chibisov, Soviet Phys. JETP Lett. **33**, 532 (1981); V. F. Mukhanov, H. A. Feldman , R. H. Brandenberger, Phys. Rept. **215**, 203 (1992). S. W. Hawking, Phys. Lett. **B115**, 295 (1982). A. H. Guth , S. Y. Pi, Phys. Rev. Lett. **49**, 1110 (1982). A. A. Starobinsky, Phys. Lett. **B117**, 175 (1982). J. M. Bardeen, P. J. Steinhardt , M. S. Turner, Phys. Rev. **D28**, 679 (1983).
- [4] C. L. Bennett *et.al.* (WMAP collaboration), Ap. J. Suppl. **148**, 1 (2003). A. Kogut *et.al.* (WMAP collaboration), Ap. J. Suppl. **148**, 161 (2003). D. N. Spergel *et. al.* (WMAP collaboration), Ap. J. Suppl. **148**, 175 (2003).
- [5] H. V. Peiris *et.al.* (WMAP collaboration), Ap. J. Suppl.**148**, 213 (2003).
- [6] D. N. Spergel *et. al.* (WMAP collaboration), astro-ph/0603449.
- [7] L. Page, *et. al.* (WMAP collaboration), astro-ph/0603450. G. Hinshaw,*et. al.* (WMAP collaboration), astro-ph/0603451. N. Jarosik, *et. al.* (WMAP collaboration), astro-ph/0603452.
- [8] M. Tegmark *et.al.* Phys. Rev **D69**,103501, (2004) D. J. Eisenstein *et.al.* ApJ. **633**, 560 (2005) U. Seljak et al., Phys. Rev. **D71**, 103515 (2005).
- [9] A. G. Sánchez *et. al.*, Mon. Not. Roy. Astron. Soc. **366**, 189 (2006). S. Cole *et.al.* Mon. Not. Roy. Astron. Soc. **362**, 505 (2005).
- [10] A. G. Sanchez and C. M. Baugh, astro-ph/0612743.
- [11] M. B. Hoffman and M. S. Turner, Phys. Rev. **64**, 023506 (2001). W. H. Kinney, Phys. Rev. **D66**,083508 (2002).
- [12] C. Savage, K. Freese and W. H. Kinney, Phys. Rev. **D 74**, 123511 (2006); L. Alabidi and D. H. Lyth, astro-ph/0510441, astro-ph/0603539; J. Martin and C. Ringeval, JCAP **0608** (2006) 009.
- [13] W. H. Kinney, E. W. Kolb, A. Melchiorri and A. Riotto, Phys.Rev. **D74** (2006) 023502.
- [14] F. Finelli, M. Rianna, N. Mandolesi, JCAP **0612**, 006 (2006). H. Peiris, R. Easther, JCAP **0610**, 017 (2006); JCAP **0607**, 002 (2006); R. Easther, H. Peiris, JCAP **0609**, 010 (2006). S. M. Leach, A. R Liddle, Phys.Rev. **D68**, 123508 (2003); Mon.Not.Roy.Astron.Soc. **341**, 1151 (2003).
- [15] D. Boyanovsky, H. J. de Vega and N. G. Sanchez, Phys. Rev. **D73**, 023008 (2006). See also ref. [22].
- [16] J. Lidsey, A. Liddle, E. Kolb, E. Copeland, T. Barreiro and M. Abney, Rev. of Mod. Phys. **69**, 373, (1997).
- [17] W. H. Kinney, A. Riotto, JCAP **0603**, 0.11 (2006); M. Giovannini, arXiv:astro-ph/0703730.
- [18] D. Cirigliano, H. J. de Vega and N. G. Sanchez, Phys. Rev. **D71**, 103518 (2005);
- [19] H. J. de Vega and N. G. Sanchez, Phys. Rev. **D74**, 063519 (2006).
- [20] C. Destri, H. J. de Vega, N. G. Sanchez, arXiv:astro-ph/0703417
- [21] A. R. Liddle, P. Parsons , J. D. Barrow, Phys. Rev. **D50**, 7222 (1994).
- [22] G. Mangano, G. Miele, C. Stornaolo, Mod.Phys.Lett.A10, 1977 (1995).
- [23] I. S. Gradshteyn and I. M. Ryzhik, Table of Integrals, Series and Products, Academic Press, 1980.
- [24] A. P. Prudnikov, Yu. A. Brichkov, O. I. Marichev, Integrals and Series, vol. 3, Nauka, Moscow, 1986.